Available online at www.sciencedirect.com
ScienceDirect
Journal of Sound and Vibration 319 (2009) 570–592
JOURNAL OF SOUND AND VIBRATION
www.elsevier.com/locate/jsvi

# Dynamic analysis of flexible linkage mechanisms under uniform temperature change

Wenfeng Hou, Xianmin Zhang*

*School of Mechanical Engineering, South China University of Technology, Guangzhou, Guangdong 510640, China*

Received 29 July 2007; received in revised form 1 May 2008; accepted 10 May 2008
Handling Editor: L.G. Tham
Available online 24 June 2008

**Abstract**

Deformation and stresses are produced not by mechanical forces alone, but by temperature variation as well. The additional stresses of a flexible mechanism caused by the temperature change should not be ignored. The generalized equations of motion for flexible linkage mechanisms, in which the thermal effects are taken into account, are developed by utilizing the virtual work method and the finite element theory in this paper. Since the determination of thermal stresses plays an important role in the design of mechanisms operating at elevated temperatures, the stress–strain relationship should include the effects of temperature. Based on the closed-form numerical algorithm, the equations are solved and the recursive scheme is proved to be efficient and converged in a few iterations for the cases examined. The Runge–Kutta method is also applied to study the transient response of the temperature change. Numerical solution results show that a small change of temperature will cause a significant change of the stresses of a flexible mechanism. The effects of temperature change should not be ignored when analyzing the dynamic performance of flexible mechanisms.


## 1. Introduction

Over the past 30 years, due to the development of high-speed machinery, robots, and aerospace structures, a considerable amount of research has addressed problems associated with the flexibility of members in flexible mechanisms. Many mechanisms are being required to run at higher speeds while maintaining greater positioning accuracy. This tendency has arisen as engineers have been challenged to design machines for increased levels of speed and accuracy subject to restrictions on weight and power requirements. However, the lighter members are more likely to elastically deform or vibrate due to the inertial and external forces. Thus, it becomes necessary to include the dynamic behavior of the mechanism system.

A number of investigators have conducted analyses of flexible mechanisms, employing both continuous and discrete systems. The importance of dynamic analysis of elastic mechanism systems has long been realized and three reviews of the research in this area may be broadly classified, based on the modeling approach, into two categories [1,2]. The first approach, which originated earlier, models the elastic links as continuous systems

*Corresponding author. Tel.: +86 20 87110059; fax: +86 20 22236360.
*E-mail address:* zhangxm@scut.edu.cn (X. Zhang).

0022-460X/$ - see front matter © 2008 Elsevier Ltd. All rights reserved.
doi:10.1016/j.jsv.2008.05.014

possessing infinite degrees of freedom [3–6]. All these works model and analyze mechanism systems which have only one elastic member and the other members are typically assumed to be rigid bodies. The links are all considered to be straight rods or beams with the exception of Badlani and Midha [7].

In the second category, the flexible links of the mechanism are modeled as discrete systems. Generally, this approach has been facilitated by the lumped parameter method [8–11] and the finite element methods [12–29]. The lumped parameter method developed by Sadler and Sandor has also been successfully implemented in the analysis of elastic mechanism. The lumped parameter method consists of modeling the continuous mass distribution of a linkage by placing a number of lumped masses at discrete locations along the linkage. Winfrey [12,13], Erdman et al. [14], and Imam et al. [15] were among the first to apply the finite element method to solve dynamic problems of the flexible mechanism systems. The finite element method provides an easier and systematic modeling technique for complex mechanisms and lays the groundwork for a general approach to the modeling of elastic mechanisms. However, in most of these works the net motion or the total motion of the system is considered to be a superposition of the rigid-body motion and the elastic motion. The rigid-body motion is treated as being governed only by kinematics and rigid-body dynamics and not influenced by the elastic motion. Some of these works address rigid-body motion and elastic motion coupling terms, but these coupling terms only represent the effect of the rigid-body motion on the elastic motion and not the effect of the elastic motion on the rigid-body motion [25–29]. Turcic and Midha [18–20] verified experimentally that the assumption that the rigid-body motion is uninfluenced by the elastic motion is valid and accurately represents mechanism systems like an elastic four-bar crank rocker mechanism with a large flywheel at the crank.

The third approach belongs to the second category. But most research works take into account the coupling between the rigid body and elastic motions, because in the area of robotics and control there exist a number of research works where manipulators with open-loop chains made up of elastic links are modeled [30–34]. Nagarajan and Turcic [32,33] allowed for the rigid-body motion and the elastic motion to influence each other, and both rigid-body degrees of freedom and the elastic degrees of freedom are considered as generalized coordinates in the derivation: these equations represent a more realistic model of a light-weight high-speed mechanism, having closed- and open-loop multi-degrees of freedom chains, and geometrically complex elastic links.

In recent years, more and more research on flexible linkage mechanisms has been reported. Most of these works refer to active vibration control [35–38], feedback control [39,40], active noise control with a piezoelectric actuator [40], optimal control [41–44], composite control [45] and simulative design [46], etc. More research on beam theories is also being carried out [47–56]. Manoach and Ribeiro [53] studied geometrically nonlinear vibrations of moderately thick beams under the combined action of mechanical and thermal loads. The results indicated that short heat pulses with high magnitudes might cause vibrations with considerably large amplitudes. Li et al. [54,55] analyzed large thermal deflections of a Timoshenko beam subjected to transversely non-uniform temperature rise by using the shooting method. His work showed that shear deformation effects became significant with a decrease of slenderness and increase of shear flexibility. Zhang and Bradford [56] described the development of a rectangular layered flat plate/shell element for the nonlinear finite element analysis of reinforced concrete slabs at elevated temperatures; the element was based on the Mindlin–Reissner plate theory and on Timoshenko's composite beam functions. The results showed that nonlinear effects were important and the finite element model incorporated geometric nonlinearity and temperature-dependent material nonlinearity under temperature loading. However, the above research did not consider the thermal effects in the dynamic flexible system, and the effects of temperature change were not taken into account in the dynamic equation of motion.

This paper is organized as follows: Section 2 processes the relationship between the total strain and the stress. Section 3 introduces the shape function with a quintic polynomial. In Section 4, the generalized equations of motion for flexible linkage mechanisms, in which the thermal effects are taken into account, are developed by utilizing the virtual work method and the finite element theory. The temperature distribution through the cross section will be assumed not to vary along the length of the element. In Section 5, based on the closed-form numerical algorithm developed by Midha et al. the equations are solved and the convergence condition is presented. The Runge–Kutta method is also applied to study the transient response of the temperature change. Numerical solution results of one linkage mechanism are presented in Section 6; both the

steady response and the transient response of the temperature change are studied, and some concluding remarks are made in Section 7.

## 2. Stress–strain relations

Deformation and stresses are produced not by mechanical forces alone, but by temperature variation as well. The additional stresses of a mechanism caused by the temperature change should not be ignored. The mechanical and thermal aspects are coupled and inseparable, which complicates the computational aspect of solving actual problems considerably. However, it is generally possible to discount the coupling and to evaluate the temperature and deformation fields separately.

The thermal strains (thermal dilatations) in an unrestrained element may be expressed as [57]

$$\varepsilon_{T_{ij}} = \delta_{ij}\alpha_T \Delta T, \quad i,j = x,y,z \tag{1}$$

where $\alpha_T$ is the coefficient of thermal expansion. For isotropic and homogeneous materials this coefficient is independent of the direction and position of the element but may depend on the temperature. $\Delta T$ is the change of temperature, $\delta_{ij}$, defined as

$$\delta_{ij} = \begin{cases} 1, & i = j, \\ 0, & i \neq j \end{cases} \tag{2}$$

If the initial strain matrix $\boldsymbol{\varepsilon}_0$ is known, the total strain matrix $\boldsymbol{e}$, including the thermal strain matrix $\boldsymbol{\varepsilon}_T$, can be expressed as [58]

$$\boldsymbol{e} = \boldsymbol{\varepsilon} + \boldsymbol{\varepsilon}_T + \boldsymbol{\varepsilon}_0 \tag{3}$$

and

$$\boldsymbol{\sigma} = \boldsymbol{D}\boldsymbol{\varepsilon} + \boldsymbol{\sigma}_0 = \boldsymbol{D}(\boldsymbol{e} - \boldsymbol{\varepsilon}_T - \boldsymbol{\varepsilon}_0) + \boldsymbol{\sigma}_0 = \boldsymbol{D}\boldsymbol{e} + \boldsymbol{D}_T\alpha_T\Delta T - \boldsymbol{D}\varepsilon_0 + \boldsymbol{\sigma}_0 \tag{4}$$

where matrix $\boldsymbol{\varepsilon}$ represents the elastic strains required to maintain continuity of displacements due to external loads and thermal and initial strains. The elastic strains are related to the stresses through Hooke's law. $\boldsymbol{D}$ is the constitutive law matrix. $\boldsymbol{\sigma}_0$ represents the residual stress matrix.

## 3. Shape function of the planar frame element

The shape function is a quintic polynomial for the lateral displacement and a linear function of the longitudinal displacement. For a two-dimensional planar frame element, there are eight displacements: longitudinal displacements $q_1$ and $q_5$, lateral displacements $q_2$ and $q_6$, elastic rotational angles $q_3$ and $q_7$, and section curvatures $q_4$ and $q_8$. The eight nodal displacements are shown in Fig. 1. The temperature distribution through the cross section will be assumed not to vary along the length of the element.

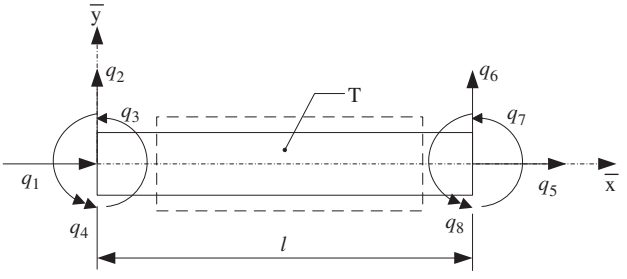


Fig. 1. Planar frame element.

According to the element finite method, the shape function can be defined as [59]

$$\boldsymbol{N}=\begin{bmatrix}\boldsymbol{N}_x\\ \boldsymbol{N}_y\end{bmatrix}=\begin{bmatrix}N_{11} & 0 & 0 & 0 & N_{15} & 0 & 0 & 0\\ 0 & N_{22} & N_{23} & N_{24} & 0 & N_{26} & N_{27} & N_{28}\end{bmatrix} \tag{5}$$

where

$$\begin{aligned}&N_{11}=1-\xi,\quad N_{22}=1-10\xi^3+15\xi^4-6\xi^5,\quad N_{23}=l(\xi-6\xi^3+8\xi^4-3\xi^5),\\ &N_{24}=\frac{l^2}{2}(\xi^2-3\xi^3+3\xi^4-\xi^5),\quad N_{15}=\xi,\quad N_{26}=10\xi^3-15\xi^4+6\xi^5\\ &N_{27}=l(-4\xi^3+7\xi^4-3\xi^5),\quad N_{28}=\frac{l^2}{2}(\xi^3-2\xi^4+\xi^5),\quad \xi=\frac{\bar{x}}{l}\end{aligned} \tag{6}$$

## 4. Formulation of equations of motion

In this study, virtual work principle is used for developing the equations of motion of the flexible mechanism systems.

Fig. 2 shows two positions of a planar frame element and the associated coordinate systems. The reference coordinate system $OXY$ is fixed to the ground. The origin of the $\overline{oxy}$ coordinate system is defined at a general point on the undeformed element, and it follows the rigid-body motion of the element. The $Oxy$ coordinate system is also attached to the ground but is rotated so that it remains parallel to the $\overline{oxy}$ system. $p$ is a general point on the undeformed element, and $p'$ is the corresponding point of $p$ on the deformed element.

The position vector $\boldsymbol{R}$, measured in the reference system, can be expressed as

$$\boldsymbol{R}=\boldsymbol{R}_0+\boldsymbol{T}_m\boldsymbol{d} \tag{7}$$

where vector $\boldsymbol{R}_0$ locates the origin of local $\overline{oxy}$ system in the reference system, vector $\boldsymbol{d}$ which is measured in the local coordinate system represents the generalized displacement (caused by the elastic deformation of the element) of point $p$. $\boldsymbol{T}_m$ is the transformation matrix between the $\overline{oxy}$ system and the reference coordinate system and depends on the gross motion of the system only. Matrix $\boldsymbol{T}_m$ is defined as [19]

$$\boldsymbol{T}_m=\begin{bmatrix}\cos\theta & -\sin\theta\\ \sin\theta & \cos\theta\end{bmatrix}$$

$$\dot{\boldsymbol{T}}_m=\dot{\theta}\begin{bmatrix}-\sin\theta & -\cos\theta\\ \cos\theta & -\sin\theta\end{bmatrix}$$

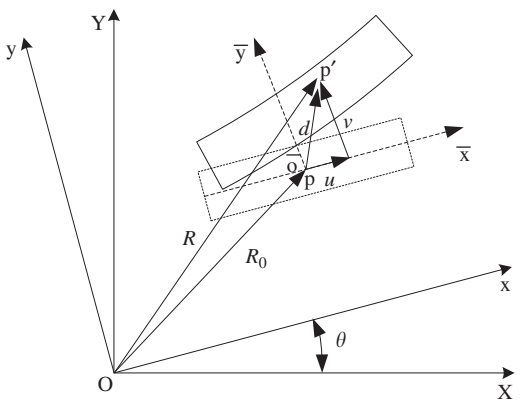


Fig. 2. Planar frame element and associated coordinate systems.

$$\ddot{\boldsymbol{T}}_m = \ddot{\theta}\begin{bmatrix} -\sin\theta & -\cos\theta \\ \cos\theta & -\sin\theta \end{bmatrix} - \dot{\theta}^2\begin{bmatrix} \cos\theta & -\sin\theta \\ \sin\theta & \cos\theta \end{bmatrix} \tag{8}$$

where $\theta$ is the angular orientation of the element.

Differentiating Eq. (7) twice with respect to time, and considering the relations

$$\boldsymbol{d} = \boldsymbol{N}\boldsymbol{q}^e \tag{9}$$

one obtains

$$\ddot{\boldsymbol{R}} = \ddot{\boldsymbol{R}}_0 + \ddot{\boldsymbol{T}}_m\boldsymbol{N}\boldsymbol{q}^e + 2\dot{\boldsymbol{T}}_m\boldsymbol{N}\dot{\boldsymbol{q}}^e + \boldsymbol{T}_m\boldsymbol{N}\ddot{\boldsymbol{q}}^e \tag{10}$$

where $\boldsymbol{d} = \{\boldsymbol{u} \quad \boldsymbol{v}\}^{\mathrm{T}}$, $\boldsymbol{q}^e = \{q_1 \quad q_2 \quad q_3 \quad q_4 \quad q_5 \quad q_6 \quad q_7 \quad q_8\}^{\mathrm{T}}$ are the nodal displacements of the element, and matrix $\boldsymbol{N}$ is the shape function described in Eqs. (5) and (6).

The principle of virtual work for the nodal system of the element can be expressed as [60]

$$\int_V \delta\boldsymbol{e}^{\mathrm{T}}\boldsymbol{\sigma}\,\mathrm{d}V = \int_V \delta\boldsymbol{d}^{\mathrm{T}}\boldsymbol{f}_b\,\mathrm{d}V + \int_S \delta\boldsymbol{d}^{\mathrm{T}}\boldsymbol{f}_s\,\mathrm{d}S + \delta\boldsymbol{q}^{e^{\mathrm{T}}}\boldsymbol{f} - \int_V \rho\delta\boldsymbol{d}^{\mathrm{T}}\ddot{\boldsymbol{d}}\,\mathrm{d}V \tag{11}$$

where $\delta\boldsymbol{d} = \boldsymbol{N}\delta\boldsymbol{q}^e$, $\delta\boldsymbol{e}$ is the total strain variation vector, $\boldsymbol{\sigma}$ the stress vector, $\delta\boldsymbol{d}$ the virtual displacement vector, $\boldsymbol{f}_b$ the actual body forces and $\boldsymbol{f}_s$ the surface forces, $\rho$ the mass density, and $\ddot{\boldsymbol{d}}$ the acceleration vector of point $p$ in the nodal system. $V$ and $S$ represent the volume and surface area of the body before deformation.

The third term on the right-hand side of Eq. (11) represents the virtual work of external forces $\boldsymbol{f}$ in moving through the corresponding virtual displacements $\delta\boldsymbol{q}^e$.

Acceleration vector $\ddot{\boldsymbol{d}}$ can be rewritten as [27]

$$\ddot{\boldsymbol{d}} = \boldsymbol{T}_m^{\mathrm{T}}\ddot{\boldsymbol{R}} \tag{12}$$

and $\ddot{\boldsymbol{R}}_0$ can be expressed as

$$\ddot{\boldsymbol{R}}_0 = \boldsymbol{T}'_m\boldsymbol{N}\ddot{\boldsymbol{q}}_0^e \tag{13}$$

Substituting Eqs. (10) and (13) into Eq. (12) yields

$$\begin{aligned}\ddot{\boldsymbol{d}} &= \boldsymbol{T}_m^{\mathrm{T}}\boldsymbol{T}'_m\boldsymbol{N}\ddot{\boldsymbol{q}}_0^e + \boldsymbol{T}_m^{\mathrm{T}}\ddot{\boldsymbol{T}}_m\boldsymbol{N}\boldsymbol{q}^e + 2\boldsymbol{T}_m^{\mathrm{T}}\dot{\boldsymbol{T}}_m\boldsymbol{N}\dot{\boldsymbol{q}}^e + \boldsymbol{T}_m^{\mathrm{T}}\boldsymbol{T}_m\boldsymbol{N}\ddot{\boldsymbol{q}}^e \\ &= \boldsymbol{N}\ddot{\boldsymbol{q}}_0^e + \boldsymbol{T}_m^{\mathrm{T}}\ddot{\boldsymbol{T}}_m\boldsymbol{N}\boldsymbol{q}^e + 2\boldsymbol{T}_m^{\mathrm{T}}\dot{\boldsymbol{T}}_m\boldsymbol{N}\dot{\boldsymbol{q}}^e + \boldsymbol{N}\ddot{\boldsymbol{q}}^e\end{aligned} \tag{14}$$

where $\ddot{\boldsymbol{q}}_0^e$ represents the generalized (absolute) rigid-body velocities of the nodal degrees of freedom of the element measured in the fixed $Oxy$coordinate system. $\boldsymbol{T}_m{}'$ is the transformation matrix from the $Oxy$ coordinate system to the $OXY$ coordinate system. Transformation matrix $\boldsymbol{T}_m{}'$ is similar to matrix $\boldsymbol{T}_m$, since the $Oxy$ system is parallel to the $\overline{oxy}$ system. The difference between the two transformation matrices is that the time derivatives of matrix $\boldsymbol{T}_m{}'$ ($\dot{\boldsymbol{T}}'_m$ and $\ddot{\boldsymbol{T}}'_m$) are equal to zero because $\boldsymbol{T}_m{}'$ is simply the transformation matrix between two fixed coordinate systems.

For the planar frame element undergoing bending, its strain has the form

$$\boldsymbol{e} = \begin{bmatrix} \dfrac{\partial\boldsymbol{u}}{\partial x} & -y\dfrac{\partial^2\boldsymbol{v}}{\partial x^2} \end{bmatrix}^{\mathrm{T}} \tag{15}$$

where $\partial\boldsymbol{u}/\partial x$ represents axial stretching and $-y(\partial^2\boldsymbol{v}/\partial x^2)$ is the strain produced by curvature $\partial^2\boldsymbol{v}/\partial x^2$.

Eq. (15) can also be expressed as

$$\boldsymbol{e} = \boldsymbol{B}\boldsymbol{q}^e \tag{16}$$

$$\delta\boldsymbol{e} = \boldsymbol{B}\delta\boldsymbol{q}^e \tag{17}$$

where

$$\boldsymbol{B} = \begin{bmatrix} \dfrac{\partial}{\partial x}\boldsymbol{N}_x & -y\dfrac{\partial^2}{\partial x^2}\boldsymbol{N}_y \end{bmatrix}^{\mathrm{T}} \tag{18}$$

Substituting Eqs. (4), (14), (16) and (17) into Eq. (11), one obtains

$$\int_V \delta \boldsymbol{e}^{\mathrm{T}} \boldsymbol{\sigma}\,\mathrm{d}V = \int_V \delta \boldsymbol{q}^{e^{\mathrm{T}}} \boldsymbol{B}^{\mathrm{T}}(\boldsymbol{D}\boldsymbol{B}\boldsymbol{q}^e + \boldsymbol{D}_T \alpha_T \Delta T - \boldsymbol{D}\boldsymbol{\varepsilon}_0 + \boldsymbol{\sigma}_0)\,\mathrm{d}V$$
$$= \delta \boldsymbol{q}^{e^{\mathrm{T}}} \int_V \boldsymbol{B}^{\mathrm{T}}\boldsymbol{D}\boldsymbol{B}\,\mathrm{d}V\boldsymbol{q}^e + \delta \boldsymbol{q}^{e^{\mathrm{T}}} \int_V \boldsymbol{B}^{\mathrm{T}}\boldsymbol{D}_T \alpha_T \Delta T\,\mathrm{d}V - \delta \boldsymbol{q}^{e^{\mathrm{T}}} \int_V \boldsymbol{B}^{\mathrm{T}}\boldsymbol{D}\boldsymbol{\varepsilon}_0\,\mathrm{d}V + \delta \boldsymbol{q}^{e^{\mathrm{T}}} \int_V \boldsymbol{B}^{\mathrm{T}}\boldsymbol{\sigma}_0\,\mathrm{d}V \quad (19)$$

$$\int_V \delta \boldsymbol{d}^{\mathrm{T}} \boldsymbol{f}_b\,\mathrm{d}V = \delta \boldsymbol{q}^{e^{\mathrm{T}}} \int_V \boldsymbol{N}^{\mathrm{T}} \boldsymbol{f}_b\,\mathrm{d}V \quad (20)$$

$$\int_S \delta \boldsymbol{d}^{\mathrm{T}} \boldsymbol{f}_s\,\mathrm{d}S = \delta \boldsymbol{q}^{e^{\mathrm{T}}} \int_S \boldsymbol{N}^{\mathrm{T}} \boldsymbol{f}_s\,\mathrm{d}S \quad (21)$$

$$\int_V \rho \delta \boldsymbol{d}^{\mathrm{T}} \ddot{\boldsymbol{d}}\,\mathrm{d}V$$
$$= \delta \boldsymbol{q}^{e^{\mathrm{T}}} \left( \int_V \rho \boldsymbol{N}^{\mathrm{T}}\boldsymbol{N}\,\mathrm{d}V\ddot{\boldsymbol{q}}_0^e + \int_V \rho \boldsymbol{N}^{\mathrm{T}}\boldsymbol{T}_m^{\mathrm{T}}\ddot{\boldsymbol{T}}_m\boldsymbol{N}\,\mathrm{d}V\boldsymbol{q}^e + 2\int_V \rho \boldsymbol{N}^{\mathrm{T}}\boldsymbol{T}_m^{\mathrm{T}}\dot{\boldsymbol{T}}_m\boldsymbol{N}\,\mathrm{d}V\dot{\boldsymbol{q}}^e + \int_V \rho \boldsymbol{N}^{\mathrm{T}}\boldsymbol{N}\,\mathrm{d}V\ddot{\boldsymbol{q}}^e \right) \quad (22)$$

With arbitrary virtual displacement $\delta \boldsymbol{q}^{e^{\mathrm{T}}}$, Eq. (11) becomes

$$\int_V \rho \boldsymbol{N}^{\mathrm{T}}\boldsymbol{N}\,\mathrm{d}V\ddot{\boldsymbol{q}}^e + 2\int_V \rho \boldsymbol{N}^{\mathrm{T}}\boldsymbol{T}_m^{\mathrm{T}}\dot{\boldsymbol{T}}_m\boldsymbol{N}\,\mathrm{d}V\dot{\boldsymbol{q}}^e + \int_V \boldsymbol{B}^{\mathrm{T}}\boldsymbol{D}\boldsymbol{B}\,\mathrm{d}V\boldsymbol{q}^e + \int_V \rho \boldsymbol{N}^{\mathrm{T}}\boldsymbol{T}_m^{\mathrm{T}}\ddot{\boldsymbol{T}}_m\boldsymbol{N}\,\mathrm{d}V\boldsymbol{q}^e$$
$$= \int_V \boldsymbol{N}^{\mathrm{T}}\boldsymbol{f}_b\,\mathrm{d}V + \int_S \boldsymbol{N}^{\mathrm{T}}\boldsymbol{f}_s\,\mathrm{d}S + \boldsymbol{f} + \int_V \boldsymbol{B}^{\mathrm{T}}\boldsymbol{D}\boldsymbol{\varepsilon}_0\,\mathrm{d}V - \int_V \boldsymbol{B}^{\mathrm{T}}\boldsymbol{\sigma}_0\,\mathrm{d}V - \int_V \boldsymbol{B}^{\mathrm{T}}\boldsymbol{D}_T\alpha_T\Delta T\,\mathrm{d}V - \int_V \rho \boldsymbol{N}^{\mathrm{T}}\boldsymbol{N}\,\mathrm{d}V\ddot{\boldsymbol{q}}_0^e \quad (23)$$

For a uniform planar frame element, the above equation can be integrated along a longitudinal orientation; then, matrices $\boldsymbol{D}$ and $\boldsymbol{D}_T$ can be expressed as

$$\boldsymbol{D} = \begin{bmatrix} E & 0 \\ 0 & E \end{bmatrix}, \quad \boldsymbol{D}_T = \begin{bmatrix} -E \\ -E \end{bmatrix} \quad (24)$$

Eq. (23) in compact form is

$$\boldsymbol{m}^e\ddot{\boldsymbol{q}}^e + 2\boldsymbol{mvel}^e\dot{\boldsymbol{q}}^e + (\boldsymbol{k}^e + \boldsymbol{macc}^e)\boldsymbol{q}^e = \boldsymbol{f}^e - \boldsymbol{f}_T^e - \boldsymbol{m}^e\ddot{\boldsymbol{q}}_0^e \quad (25)$$

where

$$\boldsymbol{m}^e = \int_V \rho \boldsymbol{N}^{\mathrm{T}}\boldsymbol{N}\,\mathrm{d}V, \boldsymbol{mvel}^e = \int_V \rho \boldsymbol{N}^{\mathrm{T}}\boldsymbol{T}_m^{\mathrm{T}}\dot{\boldsymbol{T}}_m\boldsymbol{N}\,\mathrm{d}V, \boldsymbol{k}^e = \int_V \boldsymbol{B}^{\mathrm{T}}\boldsymbol{D}\boldsymbol{B}\,\mathrm{d}V, \boldsymbol{macc}^e = \int_V \rho \boldsymbol{N}^{\mathrm{T}}\boldsymbol{T}_m^{\mathrm{T}}\ddot{\boldsymbol{T}}_m\boldsymbol{N}\,\mathrm{d}V$$
$$\boldsymbol{f}^e = \int_V \boldsymbol{N}^{\mathrm{T}}\boldsymbol{f}_b\,\mathrm{d}V + \int_S \boldsymbol{N}^{\mathrm{T}}\boldsymbol{f}_s\,\mathrm{d}S + \boldsymbol{f} + \int_V \boldsymbol{B}^{\mathrm{T}}\boldsymbol{D}\boldsymbol{\varepsilon}_0\,\mathrm{d}V - \int_V \boldsymbol{B}^{\mathrm{T}}\boldsymbol{\sigma}_0\,\mathrm{d}V, \boldsymbol{f}_T^e = \int_V \boldsymbol{B}^{\mathrm{T}}\boldsymbol{D}_T\alpha_T\Delta T\,\mathrm{d}V \quad (26)$$

Let $\boldsymbol{T}_R^{\mathrm{T}}$ represent the transformation matrix that transforms the degrees of freedom to the reference coordinate system. Let $\boldsymbol{U}^e = \{\, U_1 \quad U_2 \quad U_3 \quad U_4 \quad U_5 \quad U_6 \quad U_7 \quad U_8 \,\}^{\mathrm{T}}$ represent the new set of transformed degrees of freedom, one obtains

$$\boldsymbol{U}^e = \boldsymbol{T}_R^{\mathrm{T}}\boldsymbol{q}^e \quad (27)$$

where $\boldsymbol{U}^e$ is in the global coordinate system and $\boldsymbol{T}_R$ is defined as [33]

$$\boldsymbol{T}_R = \begin{bmatrix} \cos\theta & \sin\theta & 0 & 0 & 0 & 0 & 0 & 0 \\ -\sin\theta & \cos\theta & 0 & 0 & 0 & 0 & 0 & 0 \\ 0 & 0 & 1 & 0 & 0 & 0 & 0 & 0 \\ 0 & 0 & 0 & 1 & 0 & 0 & 0 & 0 \\ 0 & 0 & 0 & 0 & \cos\theta & \sin\theta & 0 & 0 \\ 0 & 0 & 0 & 0 & -\sin\theta & \cos\theta & 0 & 0 \\ 0 & 0 & 0 & 0 & 0 & 0 & 1 & 0 \\ 0 & 0 & 0 & 0 & 0 & 0 & 0 & 1 \end{bmatrix} \tag{28}$$

Since $\boldsymbol{T}_R$ is an orthogonal matrix, one obtains

$$\boldsymbol{q}^e = \boldsymbol{T}_R\boldsymbol{U}^e, \quad \dot{\boldsymbol{q}}^e = \boldsymbol{T}_R\dot{\boldsymbol{U}}^e + \dot{\boldsymbol{T}}_R\boldsymbol{U}^e, \quad \ddot{\boldsymbol{q}}^e = \boldsymbol{T}_R\ddot{\boldsymbol{U}}^e + 2\dot{\boldsymbol{T}}_R\dot{\boldsymbol{U}}^e + \ddot{\boldsymbol{T}}_R\boldsymbol{U}^e, \quad \ddot{\boldsymbol{q}}_0^e = \boldsymbol{T}_R\ddot{\boldsymbol{U}}_0^e \tag{29}$$

Substituting Eq. (29) into Eq. (25) and premultiplying by $\boldsymbol{T}_R^{\mathrm{T}}$ yields

$$\boldsymbol{M}^e\ddot{\boldsymbol{U}}^e + 2(\boldsymbol{MD}^e + \boldsymbol{MVEL}^e)\dot{\boldsymbol{U}}^e + (\boldsymbol{K}^e + \boldsymbol{MDD}^e + 2\boldsymbol{MDVEL}^e + \boldsymbol{MACC}^e)\boldsymbol{U}^e = \boldsymbol{Q}_f^e - \boldsymbol{Q}_T^e - \boldsymbol{M}^e\ddot{\boldsymbol{U}}_0^e \tag{30}$$

where

$$\boldsymbol{M}^e = \boldsymbol{T}_R^{\mathrm{T}}\boldsymbol{m}^e\boldsymbol{T}_R, \ \boldsymbol{MD}^e = \boldsymbol{T}_R^{\mathrm{T}}\boldsymbol{m}^e\dot{\boldsymbol{T}}_R, \ \boldsymbol{MVEL}^e = \boldsymbol{T}_R^{\mathrm{T}}\boldsymbol{mvel}^e\boldsymbol{T}_R, \boldsymbol{K}^e = \boldsymbol{T}_R^{\mathrm{T}}\boldsymbol{k}^e\boldsymbol{T}_R, \ \boldsymbol{MDD}^e = \boldsymbol{T}_R^{T}\boldsymbol{m}^e\ddot{\boldsymbol{T}}_R$$
$$\boldsymbol{MDVEL}^e = \boldsymbol{T}_R^{\mathrm{T}}\boldsymbol{mvel}^e\dot{\boldsymbol{T}}_R, \ \boldsymbol{MACC}^e = \boldsymbol{T}_R^{\mathrm{T}}\boldsymbol{macc}^e\boldsymbol{T}_R, \ \boldsymbol{Q}_f^e = \boldsymbol{T}_R^{\mathrm{T}}\boldsymbol{f}^e, \ \boldsymbol{Q}_T^e = \boldsymbol{T}_R^{\mathrm{T}}\boldsymbol{f}_T^e \tag{31}$$

Expanding Eq. (30) to the system size and combining all the element equations, we introduce the compatible matrix $\boldsymbol{T}_B$ of the coordinate system.where

$$\boldsymbol{U}^e = \boldsymbol{T}_B\boldsymbol{U}, \quad \dot{\boldsymbol{U}}^e = \boldsymbol{T}_B\dot{\boldsymbol{U}}, \quad \ddot{\boldsymbol{U}}^e = \boldsymbol{T}_B\ddot{\boldsymbol{U}}, \quad \ddot{\boldsymbol{U}}_0^e = \boldsymbol{T}_B\ddot{\boldsymbol{U}}_0 \tag{32}$$

Substituting Eq. (32) into Eq. (30) and by premultiplying $\boldsymbol{T}_B^{\mathrm{T}}$, the equations of motion for the system are stated as

$$\boldsymbol{M}\ddot{\boldsymbol{U}} + 2(\boldsymbol{MD} + \boldsymbol{MVEL})\dot{\boldsymbol{U}} + (\boldsymbol{K} + \boldsymbol{MDD} + 2\boldsymbol{MDVEL} + \boldsymbol{MACC})\boldsymbol{U} = \boldsymbol{Q}_f - \boldsymbol{Q}_T - \boldsymbol{M}\ddot{\boldsymbol{U}}_0 \tag{33}$$

where

$$\boldsymbol{M} = \sum_{i=1}^{N_e}\boldsymbol{T}_{Bi}^{\mathrm{T}}\boldsymbol{M}_i^e\boldsymbol{T}_{Bi}, \quad \boldsymbol{MD} = \sum_{i=1}^{N_e}\boldsymbol{T}_{Bi}^{\mathrm{T}}\boldsymbol{MD}_i^e\boldsymbol{T}_{Bi}, \quad \boldsymbol{MVEL} = \sum_{i=1}^{N_e}\boldsymbol{T}_{Bi}^{\mathrm{T}}\boldsymbol{MVEL}_i^e\boldsymbol{T}_{Bi}, \quad \boldsymbol{K} = \sum_{i=1}^{N_e}\boldsymbol{T}_{Bi}^{\mathrm{T}}\boldsymbol{K}_i^e\boldsymbol{T}_{Bi},$$
$$\boldsymbol{MDD} = \sum_{i=1}^{N_e}\boldsymbol{T}_{Bi}^{\mathrm{T}}\boldsymbol{MDD}_i^e\boldsymbol{T}_{Bi}, \quad \boldsymbol{MDVEL} = \sum_{i=1}^{N_e}\boldsymbol{T}_{Bi}^{\mathrm{T}}\boldsymbol{MDVEL}_i^e\boldsymbol{T}_{Bi}, \quad \boldsymbol{MACC} = \sum_{i=1}^{N_e}\boldsymbol{T}_{Bi}^{\mathrm{T}}\boldsymbol{MACC}_i^e\boldsymbol{T}_{Bi}$$
$$\boldsymbol{Q}_f = \sum_{i=1}^{N_e}\boldsymbol{T}_{Bi}^{\mathrm{T}}\boldsymbol{Q}_{fi}^e, \quad \boldsymbol{Q}_T = \sum_{i=1}^{N_e}\boldsymbol{T}_{Bi}^{\mathrm{T}}\boldsymbol{Q}_{Ti}^e \tag{34}$$

Let matrix $\boldsymbol{C}$ represent the viscous damping matrix. Incorporating the matrix damping term $\boldsymbol{C}\dot{\boldsymbol{U}}$, the equations of motion of the entire mechanism can be expressed as

$$\boldsymbol{M}\ddot{\boldsymbol{U}} + (\boldsymbol{C} + 2\boldsymbol{MD} + 2\boldsymbol{MVEL})\dot{\boldsymbol{U}} + (\boldsymbol{K} + \boldsymbol{MDD} + 2\boldsymbol{MDVEL} + \boldsymbol{MACC})\boldsymbol{U} = \boldsymbol{Q}_f - \boldsymbol{Q}_T - \boldsymbol{M}\ddot{\boldsymbol{U}}_0 \tag{35}$$

## 5. The solution of the equation of motion

Eq. (35) can be rewritten as

$$\boldsymbol{M}\ddot{\boldsymbol{U}} + \boldsymbol{C}\dot{\boldsymbol{U}} + \boldsymbol{K}\boldsymbol{U} = \boldsymbol{Q}_f - \boldsymbol{Q}_T - \boldsymbol{M}\ddot{\boldsymbol{U}}_0 - 2(\boldsymbol{MD} + \boldsymbol{MVEL})\dot{\boldsymbol{U}} - (\boldsymbol{MDD} + 2\boldsymbol{MDVEL} + \boldsymbol{MACC})\boldsymbol{U} \tag{36}$$

where $\boldsymbol{M}$, $\boldsymbol{C}$, and $\boldsymbol{K}$ represent the system mass, damping, and stiffness matrices, respectively; $\ddot{\boldsymbol{U}}$, $\dot{\boldsymbol{U}}$, $\boldsymbol{U}$, and $\ddot{\boldsymbol{U}}_0$ are the acceleration, velocity, displacement, and rigid-body acceleration, respectively, of the

degrees-of-freedom describing the mechanism system. The non-symmetric matrices $\boldsymbol{MD}$, $\boldsymbol{MVEL}$, $\boldsymbol{MDD}$, $\boldsymbol{MDVEL}$, and $\boldsymbol{MACC}$ represent coupling between the gross motion and the elastic velocity $\dot{\boldsymbol{U}}$ and the deformation $\boldsymbol{U}$, respectively.

An iteration method is presented for solving the equation of motion (36), which is expressed in a recursive form:

$$\begin{aligned}&\boldsymbol{M}\ddot{\boldsymbol{U}}^{(\lambda)}+\boldsymbol{C}\dot{\boldsymbol{U}}^{(\lambda)}+\boldsymbol{K}\boldsymbol{U}^{(\lambda)}\\&\quad=\boldsymbol{Q}_f-\boldsymbol{Q}_T-\boldsymbol{M}\ddot{\boldsymbol{U}}_0-2(\boldsymbol{MD}+\boldsymbol{MVEL})\dot{\boldsymbol{U}}^{(\lambda-1)}-(\boldsymbol{MDD}+2\boldsymbol{MDVEL}+\boldsymbol{MACC})\boldsymbol{U}^{(\lambda-1)}\end{aligned}\tag{37}$$

where subscript $\lambda$ denotes the iteration number.

In the first iteration, $\lambda=1$ and $\boldsymbol{U}^{(\lambda-1)}=\boldsymbol{U}^{(0)}=\boldsymbol{0}$, $\dot{\boldsymbol{U}}^{(\lambda-1)}=\dot{\boldsymbol{U}}^{(0)}=\boldsymbol{0}$. The following equation is solved for $\dot{\boldsymbol{U}}^{(1)}$ and $\boldsymbol{U}^{(1)}$ in each time subinterval:

$$\boldsymbol{M}\ddot{\boldsymbol{U}}^{(1)}+\boldsymbol{C}\dot{\boldsymbol{U}}^{(1)}+\boldsymbol{K}\boldsymbol{U}^{(1)}=\boldsymbol{Q}_f-\boldsymbol{Q}_T-\boldsymbol{M}\ddot{\boldsymbol{U}}_0\tag{38}$$

The convergence condition for the recursive scheme is given by

$$\left\|\boldsymbol{U}^{(\lambda)}-\boldsymbol{U}^{(\lambda-1)}\right\|_F\leqslant\varepsilon\tag{39}$$

where $\|\boldsymbol{U}\|_F$ is the Frobenius norm [61] of matrix $\boldsymbol{U}$ and $\varepsilon$ the infinitesimal positive number.

The modal analysis can be carried out based on the following equation:

$$(\boldsymbol{K}^{(\lambda-1)}-(\omega^{(\lambda-1)})^2\boldsymbol{M}^{(\lambda-1)})\boldsymbol{\Phi}^{(\lambda-1)}=\boldsymbol{0}\tag{40}$$

where $\boldsymbol{\Phi}$ denotes mode shapes, and

$$\boldsymbol{U}^{(\lambda)}=\boldsymbol{\Phi}^{(\lambda-1)}\boldsymbol{\eta}^{(\lambda)},\quad\dot{\boldsymbol{U}}^{(\lambda)}=\boldsymbol{\Phi}^{(\lambda-1)}\dot{\boldsymbol{\eta}}^{(\lambda)},\quad\ddot{\boldsymbol{U}}^{(\lambda)}=\boldsymbol{\Phi}^{(\lambda-1)}\ddot{\boldsymbol{\eta}}^{(\lambda)}\tag{41}$$

$$(\boldsymbol{\Phi}^{(i)})^{\mathrm{T}}MF^{(j)}=\begin{cases}1, & i=j,\\ 0, & i\neq j,\end{cases}\quad(\boldsymbol{\Phi}^{(i)})^{\mathrm{T}}\boldsymbol{M}\boldsymbol{\Phi}^{(j)}=\begin{cases}\omega_i^2, & i=j,\\ 0, & i\neq j\end{cases}\tag{42}$$

Substituting Eqs. (41) into Eq. (37) and premultiplying by $(\boldsymbol{\Phi}^{(\lambda-1)})^{\mathrm{T}}$, one obtains

$$\ddot{\boldsymbol{\eta}}_r^{(\lambda)}+2\zeta_r\omega_r^{(\lambda-1)}\dot{\boldsymbol{\eta}}_r^{(\lambda)}+(\omega_r^{(\lambda-1)})^2\boldsymbol{\eta}_r^{(\lambda)}=\boldsymbol{N}_{f_r}-\boldsymbol{N}_{c_r}\dot{\boldsymbol{\eta}}_r^{(\lambda-1)}-\boldsymbol{N}_{k_r}\boldsymbol{\eta}_r^{(\lambda-1)}\quad(r=1,2,\ldots,n_r)\tag{43}$$

where $\zeta_r$ is the damping ratio of the $r$th mode, $n_r$ is the number of truncated modes, $\boldsymbol{\eta}$ is the vector of modal coordinates associated with $\boldsymbol{\Phi}$, and

$$\begin{aligned}\boldsymbol{N}_f&=(\boldsymbol{\Phi}^{(\lambda-1)})^{\mathrm{T}}(\boldsymbol{Q}_f-\boldsymbol{Q}_T-\boldsymbol{M}\ddot{\boldsymbol{U}}_0)\\\boldsymbol{N}_c&=2(\boldsymbol{\Phi}^{(\lambda-1)})^{\mathrm{T}}(\boldsymbol{MD}+\boldsymbol{MVEL})\boldsymbol{\Phi}^{(\lambda-1)}\\\boldsymbol{N}_k&=(\boldsymbol{\Phi}^{(\lambda-1)})^{\mathrm{T}}(\boldsymbol{MDD}+2\boldsymbol{MDVEL}+\boldsymbol{MACC})\boldsymbol{\Phi}^{(\lambda-1)}\end{aligned}\tag{44}$$

A closed-form numerical algorithm developed by Midha and Erdmann [62] was used to solve Eqs. (43); the recursive scheme is proved to be efficient and converged in a few iterations for the cases examined.

The above method is mainly used in the condition of steady state, but for the transient state, Eqs. (43) can be solved by the Runge–Kutta method. Eqs. (43) can be rewritten as

$$\ddot{\boldsymbol{\eta}}(t_i)+(\bar{\boldsymbol{C}}(t_i)+\boldsymbol{N}_c(t_i))\dot{\boldsymbol{\eta}}(t_i)+(\boldsymbol{\Omega}^2(t_i)+\boldsymbol{N}_k(t_i))\boldsymbol{\eta}(t_i)=\boldsymbol{N}_f(t_i)\tag{45}$$

where

$$\bar{\boldsymbol{C}}(t_i)=\begin{bmatrix} 2\zeta_1(t_i)\omega_1(t_i) & 0 & \cdots & 0 \\ 0 & 2\zeta_2(t_i)\omega_2(t_i) & \cdots & 0 \\ \vdots & \vdots & \ddots & \vdots \\ 0 & 0 & \cdots & 2\zeta_{n_r}(t_i)\omega_{n_r}(t_i) \end{bmatrix}_{n_r\times n_r}$$

$$\boldsymbol{\Omega}^2=\begin{bmatrix} \omega_1^2(t_i) & 0 & \cdots & 0 \\ 0 & \omega_2^2(t_i) & \cdots & 0 \\ \vdots & \vdots & \ddots & \vdots \\ 0 & 0 & \cdots & \omega_{n_r}^2(t_i) \end{bmatrix}_{n_r\times n_r}$$

$$\omega_1(t_i)<\omega_2(t_i)<\cdots<\omega_{n_r}(t_i)$$

where $t_i$ is the $i$th time subintervals.

Let $\boldsymbol{X}_1=\boldsymbol{\eta}$, $\boldsymbol{X}_2=\dot{\boldsymbol{\eta}}$.

Eq. (45) can be expressed as

$$\begin{Bmatrix} \dfrac{\mathrm{d}\boldsymbol{X}_1(t_i)}{\mathrm{d}t} \\ \dfrac{\mathrm{d}\boldsymbol{X}_2(t_i)}{\mathrm{d}t} \end{Bmatrix}=\begin{bmatrix} \boldsymbol{0}_{n_r\times 1} \\ \boldsymbol{N}_f(t_i)_{n_r\times 1} \end{bmatrix}+\begin{bmatrix} \boldsymbol{0}_{n_r\times n_r} & \boldsymbol{E}_{n_r\times n_r} \\ -(\boldsymbol{\Omega}^2(t_i)+\boldsymbol{N}_k(t_i))_{n_r\times n_r} & -(\bar{\boldsymbol{C}}(t_i)+\boldsymbol{N}_c(t_i))_{n_r\times n_r} \end{bmatrix}\begin{Bmatrix} \boldsymbol{X}_1(t_i) \\ \boldsymbol{X}_2(t_i) \end{Bmatrix} \tag{46}$$

where $\boldsymbol{E}$ is the identity matrix, and

$$\boldsymbol{X}_1(t_i)=\{\boldsymbol{\eta}_1(t_i),\boldsymbol{\eta}_2(t_i),\ldots,\boldsymbol{\eta}_{n_r}(t_i)\}^{\mathrm{T}},\quad X_2(t_i)=\{\dot{\boldsymbol{\eta}}_1(t_i),\dot{\boldsymbol{\eta}}_2(t_i),\ldots,\dot{\boldsymbol{\eta}}_{n_r}(t_i)\}^{\mathrm{T}}$$

The Runge–Kutta method is proved to be efficient in the following cases.

## 6. Numerical result

To verify the thermal effect under a uniform temperature change, one linkage mechanism is studied. Fig. 3 illustrates the basic configuration of an actual four-bar linkage mechanism. The parameters defining the mechanism are listed in Table 1. It is constructed of aluminum strips; for the link dimensions chosen, each of the members may be treated as a slender beam and modeled with beam finite elements. The crank runs at six different speeds, from slow to a reasonably high speed (200–600 rev/min). In the analytical model, a total of 10 elements are employed, the crank is divided into two elements, while the coupler and the follower are both divided into four elements. The fundamental time period is divided into 128 equal time subintervals.

It is assumed that the temperature of the mechanism is a function of time. Fig. 4 shows the curve of the temperature versus the time [63]. The initial temperature is 20 °C, and it increases nonlinearly to 28.2 °C in 15 s.

The function between the temperature and the time can be established by the curve fitting method. In this paper, a sextic polynomial is employed in order to have the best fit for the curve of Fig. 4, which can be expressed as

$$T(t)=\begin{cases} a_0+a_1t+a_2t^2+a_3t^3+a_4t^4+a_5t^5+a_6t^6, & 0\leqslant t\leqslant 15\,\mathrm{s}, \\ a_0+a_1t_s+a_2t_s^2+a_3t_s^3+a_4t_s^4+a_5t_s^5+a_6t_s^6, & \text{when } t>15\,\mathrm{s},\ \text{then } t_s=15\,\mathrm{s} \end{cases} \tag{47}$$

where

$$a_0=20,\quad a_1=3.90212415700095,\quad a_2=-0.871130281057564,\quad a_3=0.112740167433368,$$
$$a_4=-0.00859429768001374,\quad a_5=0.000355360208944467,\quad a_6=-6.11226105887796\times 10^{-6}$$

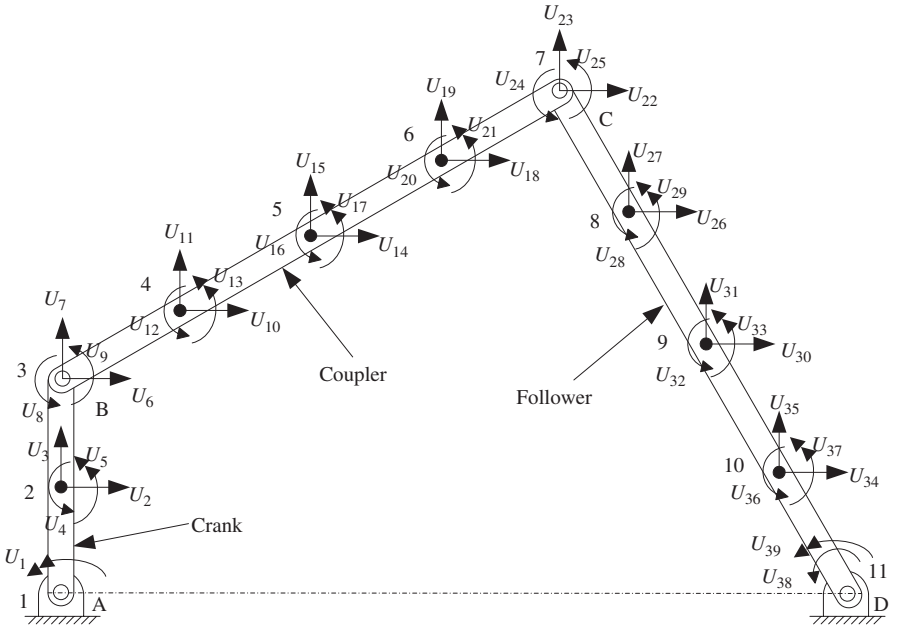


Fig. 3. Four-bar mechanism.

Table 1
Four-bar mechanism parameters

| Parameter | Crank | Coupler | Follower |
|---|---|---|---|
| Length (mm) | 98.8 | 302 | 300 |
| Width (mm) | 25 | 25 | 25 |
| Thickness (mm) | 3 | 3 | 3 |
| Distance between ground pivots (mm) | | 332.2 | |
| Lumped mass of the bearing assembly at the crank-coupler connection (kg) | | 0.1308 | |
| Lumped mass of the bearing assembly at the coupler-follower connection (kg) | | 0.113 | |
| Modulus of elasticity (Pa) | | $7.102 \times 10^{10}$ | |
| Weight density (kg/m$^3$) | | 2712 | |
| The coefficient of thermal expansion $\alpha_T$ (K$^{-1}$) | | $23 \times 10^{-6}$ | |

Now we will study both the transient responses and the steady responses of the mechanism to the temperature changes at six different speeds.

Firstly, we study the transient response to the temperature changes according to the curve shown in Fig. 4. In order to study the transient response of the mechanism to the temperature changes at six different crank speeds, the transient time is divided into different equal fundamental time segments (50, 75, 100, 125, and 150, respectively) and each fundamental time period is also divided into 128 equal time subintervals. Hence in each time subintervals one can use the Runge–Kutta method to study the transient response of the system.

Figs. 5–24 show the transient responses of the stresses at the coupler midpoint and the follower midpoint of the mechanisms at six different crank speeds. Figs. 7, 8, 11, 12, 15, 16, 19, 20, 23 and 24 show the transient responses of the stresses in the first 5 s. The temperature of the mechanism follows Fig. 4. From Fig. 4, one finds that the temperature changes very fast in the first 0–5 s, and then changes slowly in the following 5–15 s. From Figs. 5–24, one finds that the changes of stresses are nonlinear and depend on the changes of the temperature. The stresses also change fast in the first 0–5 s, and then change slowly in the following 5–15 s. When the temperature reaches a steady state (the time is more than 15 s), the change of the stresses also becomes steady.

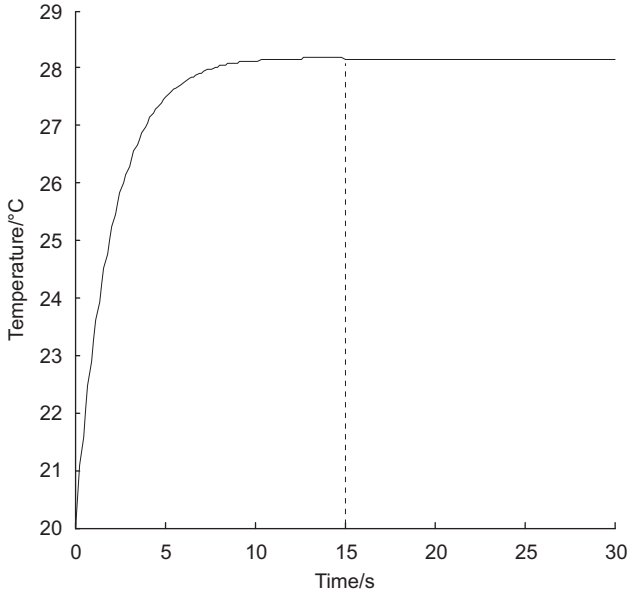


Fig. 4. The change of the temperature.

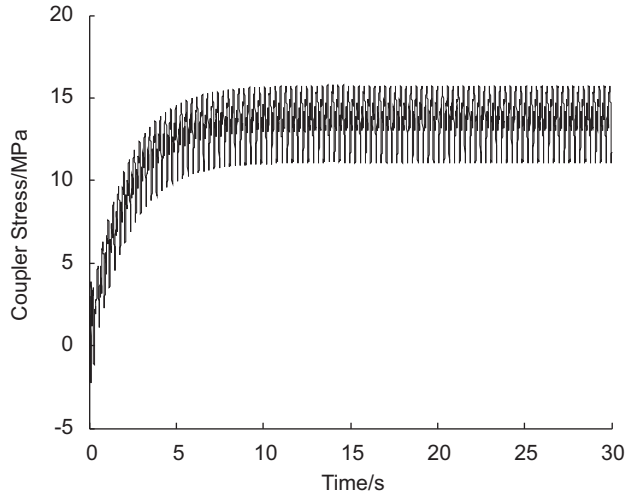


Fig. 5. Stresses at the coupler midpoint in 30 s at a crank speed of 200 rev/min.

Secondly, we study the steady-state response of the mechanism to different temperature changes. Here we will compare stresses both at the coupler midpoint and at the follower midpoint between the analytical results of Ref. [18] not taking into account the thermal effects and the present method taking into account the thermal effects under different temperature changes at six different crank speeds.

Table 2 shows the absolute maximum stresses of the coupler midpoint under different temperature changes at six different crank speeds. Table 3 shows the absolute maximum stresses of the follower midpoint under different temperature changes at six different crank speeds, and the change of temperature 0 °C is the analytical results of Ref. [18] not taking into account the thermal effects. From Tables 2 and 3, one finds that the more the temperature rise or decrease, the more significant the absolute maximum stresses both at the coupler midpoint and at the follower midpoint. Under the same temperature change, the absolute maximum

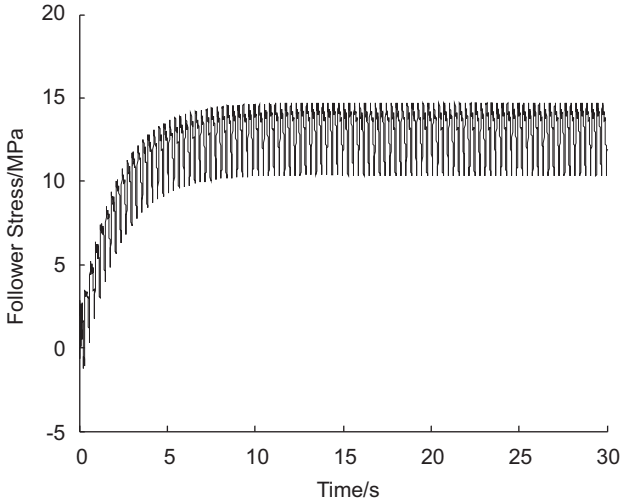


Fig. 6. Stresses at the follower midpoint in 30 s at a crank speed of 200 rev/min.

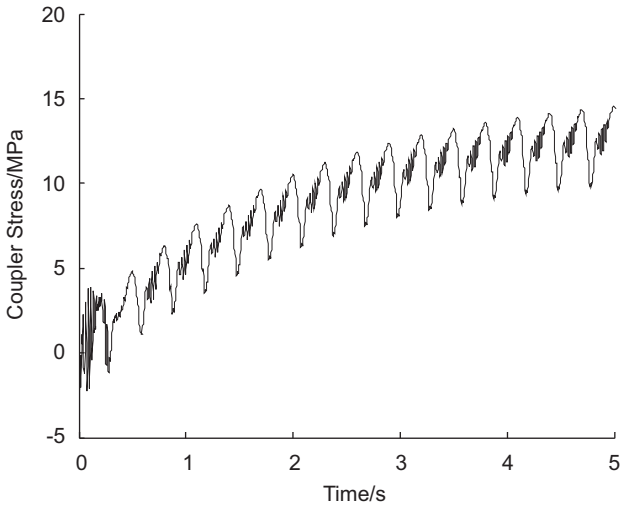


Fig. 7. Stresses at the coupler midpoint in 0–5 s at a crank speed of 200 rev/min.

stresses both at the coupler midpoint and at the follower midpoint are different at six different crank speeds. Under the same temperature change, the higher the crank speed, the larger the maximum stresses are.

To illustrate the thermal effects under a uniform temperature change in the steady state, here we mainly study the response of the mechanism at a crank speed of 400 rev/min.

The dashed line in Fig. 25 indicates stresses at the coupler midpoint of the analytical results of Ref. [18] not taking into account the thermal effects, and the solid line represents the analytical results of the present method taking into account the thermal effects under the change of temperature 1 °C. The absolute maximum stress of the analytical results of Ref. [18] at the coupler midpoint is 18.13 MPa, while the absolute maximum stress of the analytical results of the present method is 19.81 MPa. The absolute maximum difference value between the two lines in Fig. 25 is 1.70 MPa, while the absolute minimum value is 1.62 MPa.

The dashed line in Fig. 26 indicates stresses at the follower midpoint of the analytical results of Ref. [18] not taking into account the thermal effects, and the solid line represents the analytical results of the present method taking into account the thermal effects under the change of temperature 1 °C. The absolute maximum stress of the analytic results of Ref. [18] at the follower is 15.92 MPa, while the absolute maximum stress of the

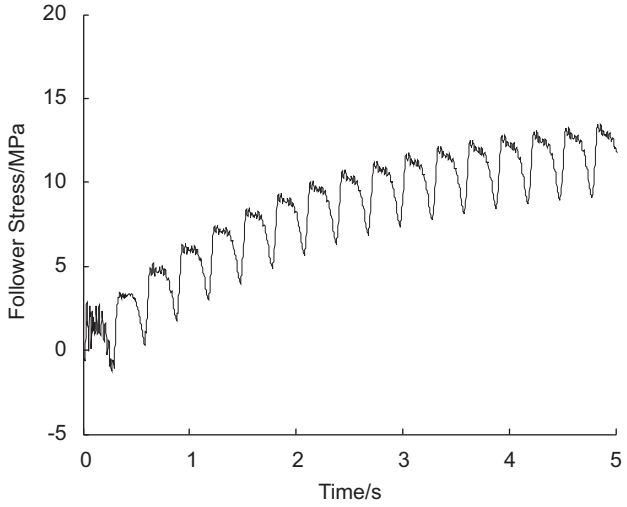


Fig. 8. Stresses at the follower midpoint in 0–5 s at a crank speed of 200 rev/min.

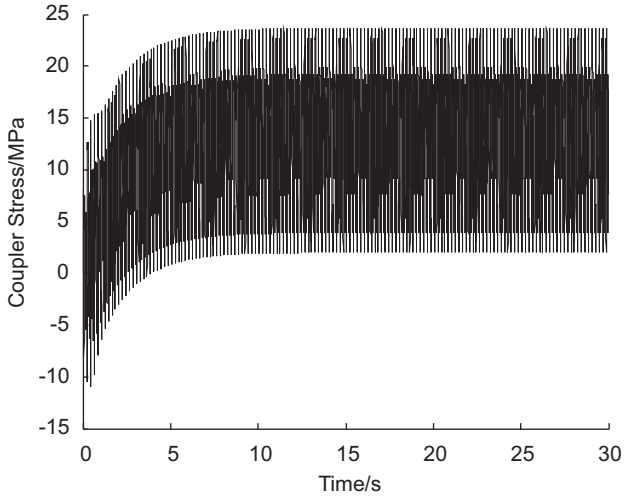


Fig. 9. Stresses at the coupler midpoint in 30 s at a crank speed of 300 rev/min.

analytical results of the present method is 14.33 MPa. The absolute maximum difference value between the two lines in Fig. 26 is 1.64 MPa, while the absolute minimum value is 1.59 MPa.

Fig. 27 shows stresses at the coupler midpoint under the effects of temperature changes −10, −5, −1, 0, 1, 5, and 10 °C, and the line under the temperature change 0 °C represents the analytical results of Ref. [18] not taking into account the thermal effects. The absolute maximum stress of each analytical results shown in Fig. 27 is 31.10, 22.92, 16.44, 18.13, 19.81, 26.54, and 34.96 MPa, respectively. The absolute maximum difference values between the results of Ref. [18] and the present method are 17.02, 8.51, 1.70, 1.70, 8.51, and 17.02 MPa, respectively; while the absolute minimum difference values are 16.16, 8.08, 1.62, 1.62, 8.08, and 16.16 MPa, respectively.

Fig. 28 shows stresses at the follower midpoint under the effects of temperature changes −10, −5, −1, 0, 1, 5 and 10 °C, and the line under the temperature change 0 °C represents the analytical results of Ref. [18] not taking into account the thermal effects. The absolute maximum stress of each analytical results shown in

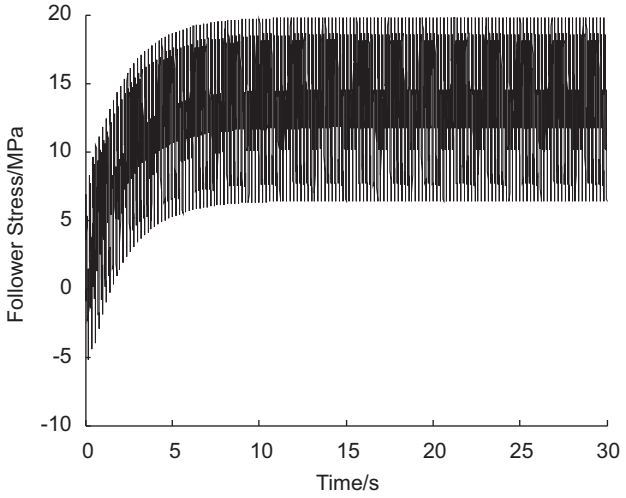


Fig. 10. Stresses at the follower midpoint in 30 s at a crank speed of 300 rev/min.

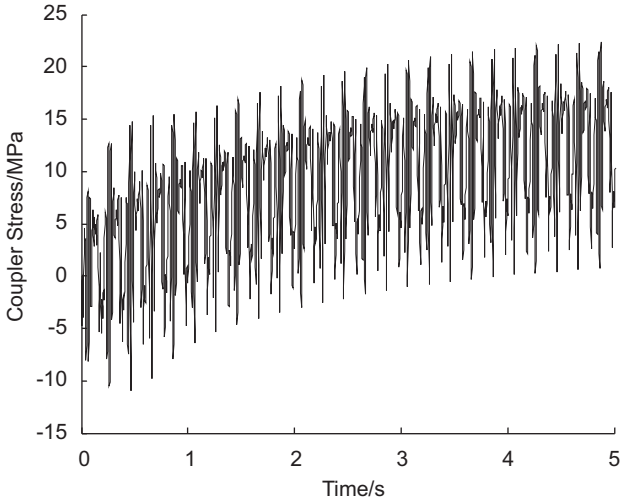


Fig. 11. Stresses at the coupler midpoint in 0–5 s at a crank speed of 300 rev/min.

Fig. 28 is 31.88, 23.90, 17.52, 15.92, 14.33, 19.83, and 27.98 MPa, respectively. The absolute maximum value between the results of Ref. [18] and the present method is 16.36, 8.18, 1.64, 1.64, 8.18, and 16.36 MPa, respectively, while the absolute minimum value is 15.86, 7.93, 1.59, 1.59, 7.93, and 15.86 MPa, respectively.

The results of Figs. 25–28 indicate that a small change of temperature will cause a significant change of the stresses of the flexible mechanism at a crank speed of 400 rev/min. It was also found that the thermal effect also causes significant responses under a uniform temperature change at the other crank speeds. It is found that the more the temperature rise or decrease, the more significant the absolute maximum difference values and the absolute minimum difference values between the results of Ref. [18] and the present method both at the coupler midpoint and at the follower midpoint. In the steady state, the absolute maximum difference values or the absolute minimum difference values almost keep linearly increasing or decreasing under different temperature changes at the same crank speed. Under the same temperature change, the absolute maximum difference values remain almost the same at six different crank speeds, and so do the absolute minimum difference values. The results of Figs. 5–28 and Tables 2 and 3 indicate that a small change of temperature will cause a significant change of the stresses of a flexible mechanism and whether the stresses increase or decrease

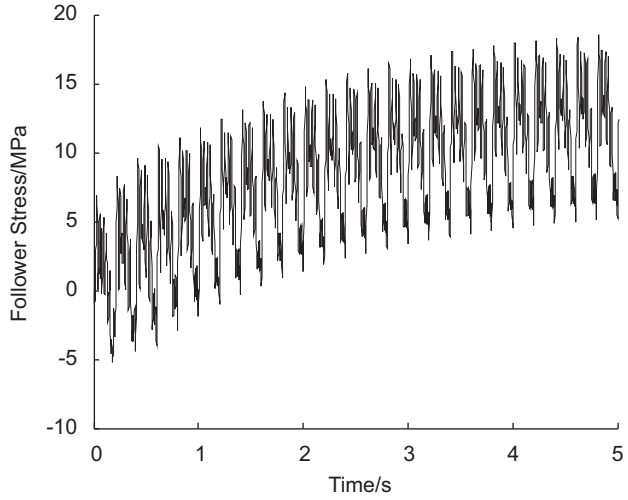


Fig. 12. Stresses at the follower midpoint in 0–5 s at a crank speed of 300 rev/min.

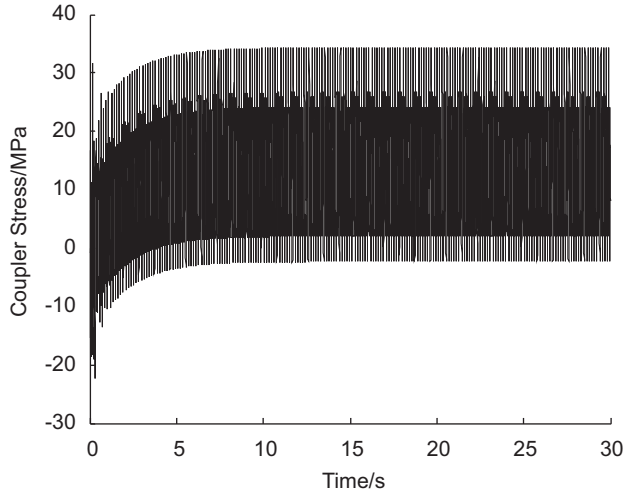


Fig. 13. Stresses at the coupler midpoint in 30 s at a crank speed of 400 rev/min.

linearly or nonlinearly depend on the change of temperature. The effects of temperature change should not be ignored when analyzing the dynamic motion of flexible mechanisms.

## 7. Summary and conclusions

The generalized equations of motion for flexible linkage mechanisms, in which the thermal effects and elastic deformation are taken into account, are derived by utilizing the virtual work method and the finite element theory in this paper. Based on the closed-form numerical algorithm, the equations are solved and the recursive scheme is proved to be efficient and converged in a few iterations for the cases examined. The Runge–Kutta method is also applied to study the transient response of the temperature change.

Numerical solution results of a flexible linkage mechanism indicate that: (1) a small change of temperature will cause a significant change of the stresses of a flexible mechanism. (2) The more the temperature rise or decrease, the more significant the stresses of a flexible mechanism. (3) Whether the stresses increase or decrease linearly or nonlinearly depends on the function of the temperature to the time during the transient response

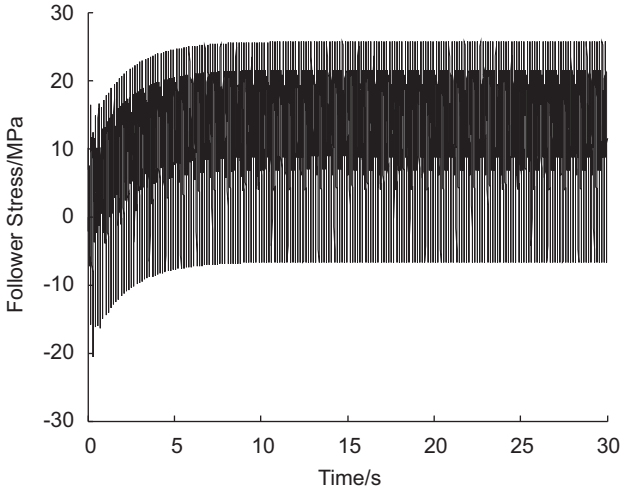


Fig. 14. Stresses at the follower midpoint in 30 s at a crank speed of 400 rev/min.

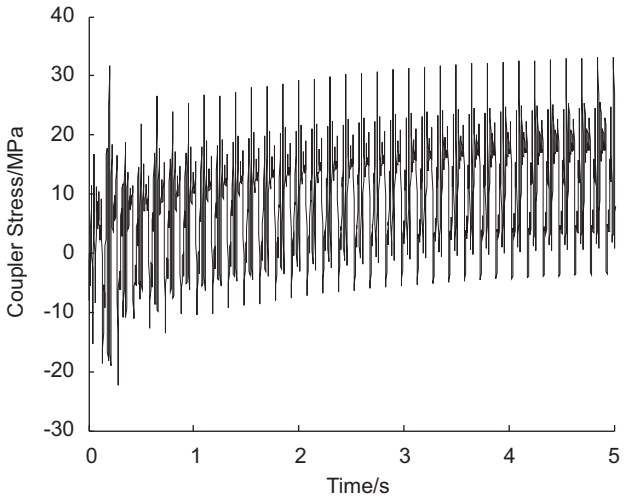


Fig. 15. Stresses at the coupler midpoint in 0–5 s at a crank speed of 400 rev/min.

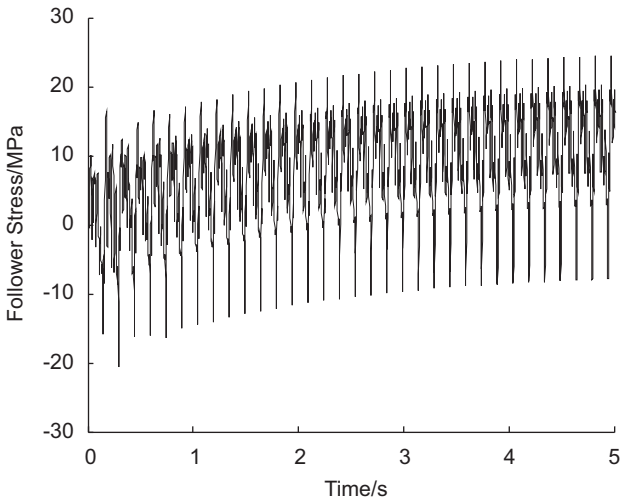


Fig. 16. Stresses at the follower midpoint in 0–5 s at a crank speed of 400 rev/min.

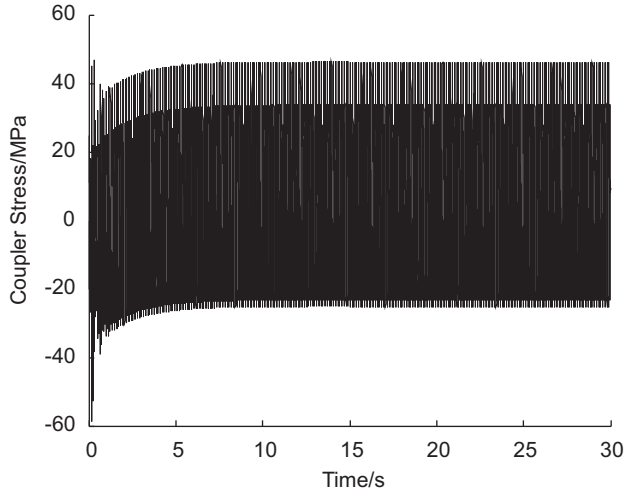


Fig. 17. Stresses at the coupler midpoint in 30 s at a crank speed of 500 rev/min.

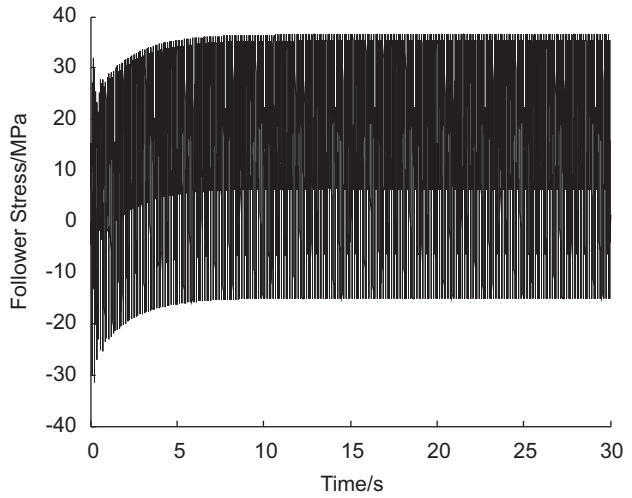


Fig. 18. Stresses at the follower midpoint in 30 s at a crank speed of 500 rev/min.

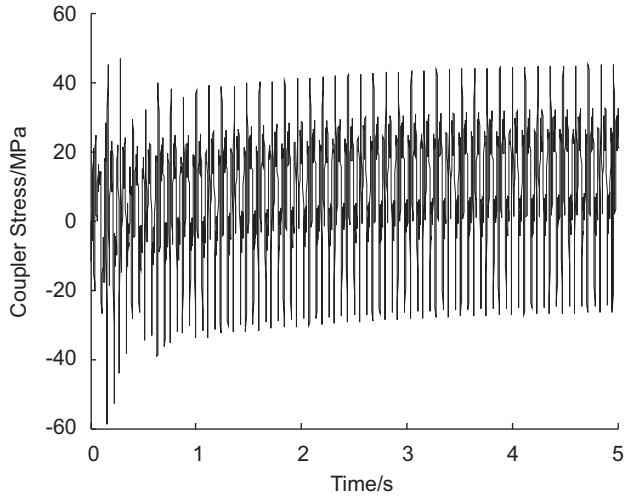


Fig. 19. Stresses at the coupler midpoint in 0–5 s at a crank speed of 500 rev/min.

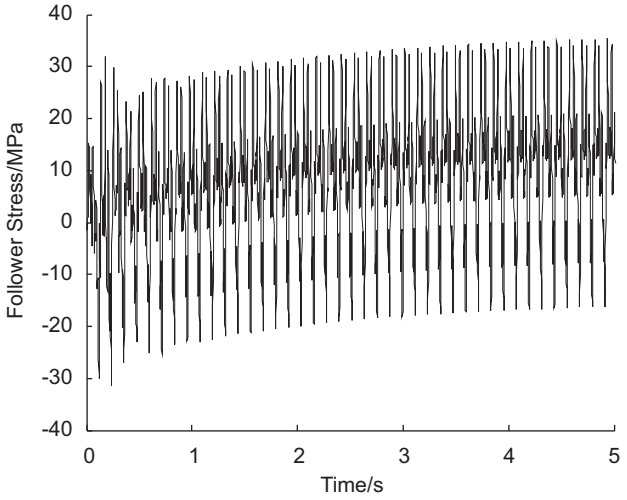


Fig. 20. Stresses at the follower midpoint in 0–5 s at a crank speed of 500 rev/min.

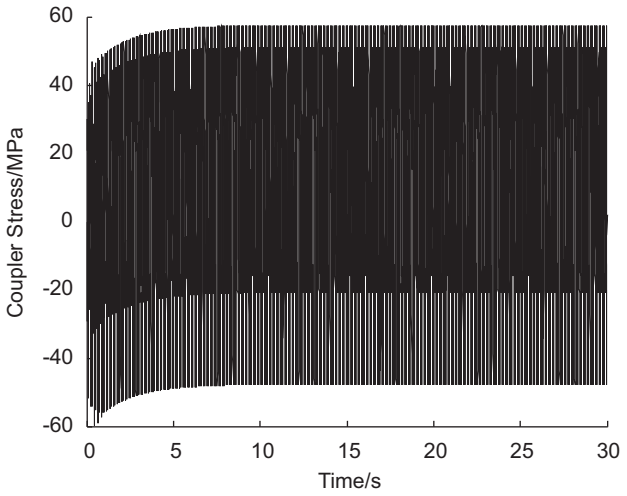


Fig. 21. Stresses at the coupler midpoint in 30 s at a crank speed of 600 rev/min.

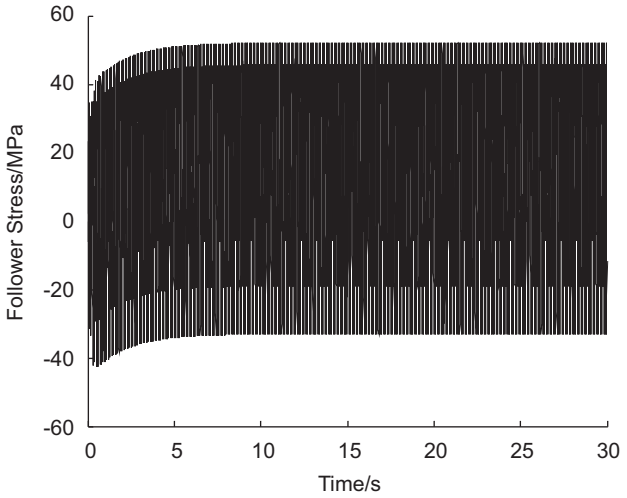


Fig. 22. Stresses at the follower midpoint in 30 s at a crank speed of 600 rev/min.

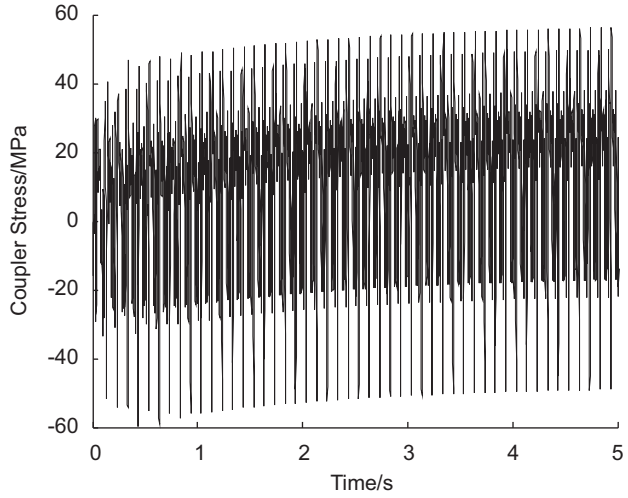


Fig. 23. Stresses at the coupler midpoint in 0–5 s at a crank speed of 600 rev/min.

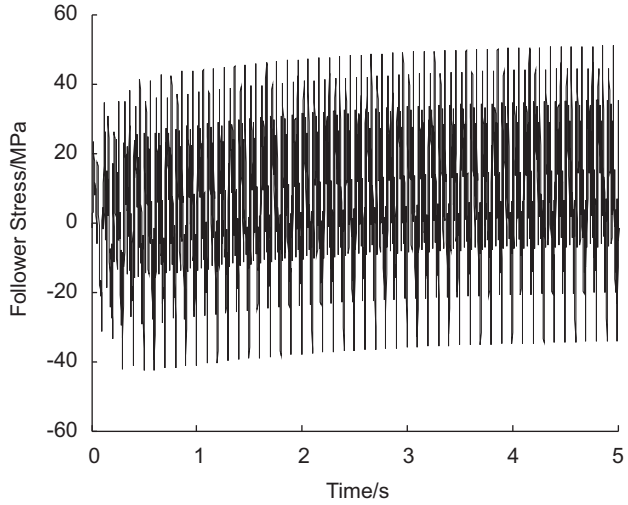


Fig. 24. Stresses at the follower midpoint in 0–5 s at a crank speed of 600 rev/min.

Table 2
The absolute maximum stresses of the coupler midpoint under different temperature changes at six different crank speeds

| Change of temperature, $\Delta T$ (°C) | The absolute maximum stresses of the coupler midpoint (MPa) | | | | |
|---|---|---|---|---|---|
| | 200 rev/min | 300 rev/min | 400 rev/min | 500 rev/min | 600 rev/min |
| −10 | 18.66 | 24.25 | 31.10 | 54.96 | 65.51 |
| −5 | 10.54 | 15.86 | 22.92 | 46.65 | 57.24 |
| −1 | 4.04 | 9.15 | 16.44 | 40.00 | 50.63 |
| 0 | 2.42 | 7.47 | 18.13 | 38.34 | 48.98 |
| 1 | 3.54 | 9.14 | 19.81 | 36.68 | 47.33 |
| 5 | 10.33 | 15.85 | 26.54 | 37.08 | 42.69 |
| 10 | 18.82 | 24.23 | 34.96 | 45.46 | 51.15 |

Table 3
The absolute maximum stresses of the follower midpoint under different temperature changes at six different crank speeds

| Change of temperature, $\Delta T$ (°C) | The absolute maximum stresses of the follower midpoint (MPa) | | | | |
|---|---|---|---|---|---|
| | 200 rev/min | 300 rev/min | 400 rev/min | 500 rev/min | 600 rev/min |
| −10 | 18.47 | 21.22 | 31.88 | 42.62 | 49.43 |
| −5 | 10.47 | 13.21 | 23.90 | 34.64 | 41.49 |
| −1 | 4.07 | 6.83 | 17.52 | 28.25 | 35.14 |
| 0 | 2.47 | 5.71 | 15.92 | 26.66 | 33.55 |
| 1 | 3.07 | 7.34 | 14.33 | 25.06 | 31.96 |
| 5 | 9.58 | 13.84 | 19.83 | 29.68 | 37.19 |
| 10 | 17.72 | 21.96 | 27.98 | 37.81 | 45.34 |

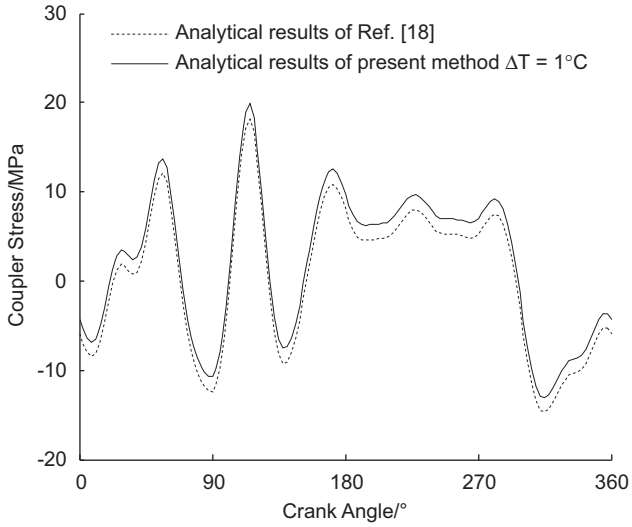


Fig. 25. Stresses at the coupler midpoint as a function of crank angle at a crank speed of 400 rev/min.

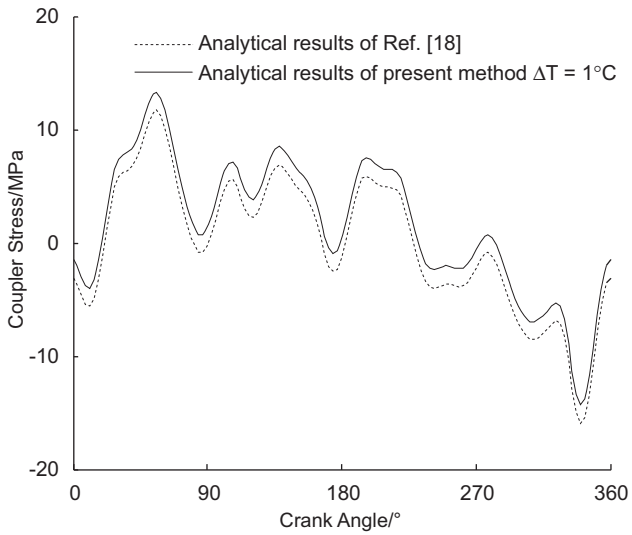


Fig. 26. Stresses at the follower midpoint as a function of crank angle at a crank speed of 400 rev/min.

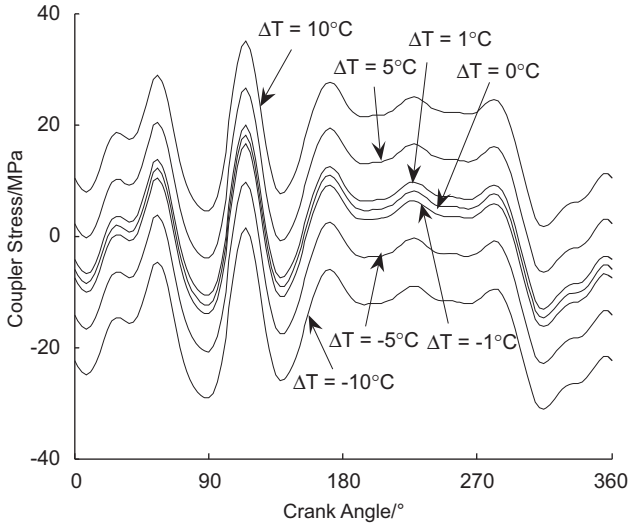


Fig. 27. Stresses at the coupler midpoint under different temperature changes at a crank speed of 400 rev/min.

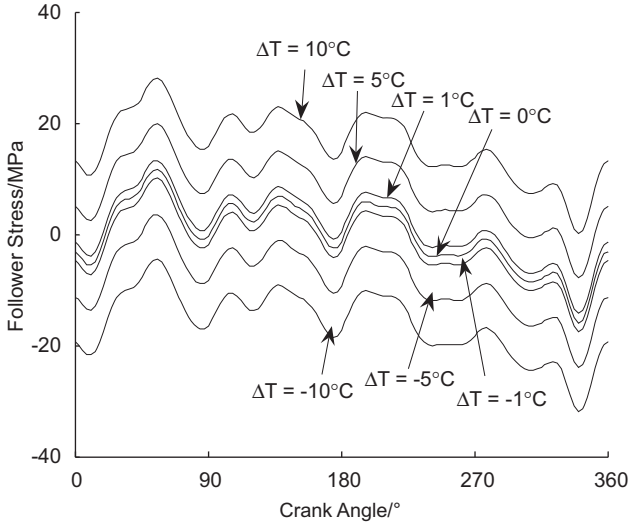


Fig. 28. Stresses at the follower midpoint under different temperature changes at a crank speed of 400 rev/min.

same as the stresses increasing or decreasing linearly during the steady response under uniform temperature change. (4) Under the same temperature change, the higher the crank speed, the larger the maximum stresses.

The effects of temperature change should not be ignored when analyzing the dynamic performance of a flexible mechanism.

## Acknowledgments

This research was supported by the National Natural Science Foundation of China (50775073); the Guangzhou technology project (2006A10401004); the Guangdong Hong Kong Technology Cooperation Funding (Dongguan Project 20061682); and the Research Project of Ministry of Education and Guangdong Province (2006D90304001). The support is gratefully acknowledged.

## References


[1] A.G. Erdman, G.N. Sandor, Kineto-elastodynamics–a review of the state of the art and trends, *Mechanism and Machine Theory* 7 (1) (1972) 19–33.

[2] G.G. Lowen, C.C. Chassapis, The elastic behavior of linkages: an update, *Mechanism and Machine Theory* 21 (1) (1986) 33–42.

[3] P.W. Jasinski, H.C. Lee, G.N. Sandor, Vibration of elastic connecting rod of a high-speed slider-crank mechanism, *ASME Journal of Engineering for Industry* 93 (3) (1971) 636–644.

[4] S.C. Chu, K.C. Pan, Dynamic response of high-speed slider-crank mechanism with an elastic connecting rod, *ASME Journal of Engineering for Industry* 97 (2) (1975) 542–549.

[5] M. Badlani, W. Kleinhenz, Dynamic stability of elastic mechanisms, *ASME Journal of Mechanical Design* 101 (2) (1979) 149–153.

[6] I.G. Tadjhakhsh, Stability of motion of elastic planar linkage with application to slider crank mechanism, *ASME Journal of Mechanical Design* 104 (4) (1982) 698–703.

[7] M. Badlani, A. Midha, Member initial curvature effects on the elastic slider-crank mechanism response, *ASME Journal of Mechanical Design* 104 (1) (1982) 159–167.

[8] J.P. Sadler, G.N. Sandor, A lumped parameter approach to vibration and stress analysis of elastic linkages, *ASME Journal of Engineering for Industry* 95 (2) (1973) 549–557.

[9] J.P. Sadler, G.N. Sandor, Nonlinear vibration analysis of elastic four-bar linkage, *ASME Journal of Engineering for Industry* 96 (2) (1974) 411–419.

[10] J.P. Sadler, G.N. Sandor, On the analytical lumped-mass model of an elastic four-bar mechanism, *ASME Journal of Engineering for Industry* 97 (2) (1975) 561–565.

[11] E.P. Golebiewski, J.P. Sadler, Analytical and experimental investigation of elastic slider-crank mechanisms, *ASME Journal of Engineering for Industry* 98 (4) (1976) 1266–1271.

[12] R.C. Winfrey, Elastic link mechanism dynamics, *ASME Journal of Engineering for Industry* 93 (1) (1971) 268–272.

[13] R.C. Winfrey, Dynamic analysis of elastic link mechanisms by reduction of coordinate, *ASME Journal of Engineering for Industry* 94 (2) (1972) 577–581.

[14] A.G. Erdman, G.N. Sandor, R.G. Oakberg, A general method for kineto-elastodynamic analysis and synthesis of mechanisms, *ASME Journal of Engineering for Industry* 94 (4) (1972) 1193–1205.

[15] I. Imam, G.N. Sandor, S.N. Kramer, Deflection and stress analysis in high-speed planar mechanisms with elastic links, *ASME Journal of Engineering for Industry* 95 (2) (1973) 541–548.

[16] A. Midha, A.G. Erdman, D.A. Frohrib, Finite element approach to mathematical modeling of high-speed elastic linkages, *Mechanism and Machine Theory* 13 (6) (1978) 603–618.

[17] W.L. Cleghorn, B. Taborrok, R.G. Fenton, Finite element analysis of high-speed flexible mechanisms, *Mechanism and Machine Theory* 16 (4) (1981) 407–424.

[18] D.A. Turcic, A. Midha, Generalized equations of motion for the dynamic analysis of elastic mechanism systems, *ASME Journal of Dynamic Systems, Measurements, and Control* 106 (4) (1984) 243–248.

[19] D.A. Turcic, A. Midha, Dynamic analysis of elastic mechanism systems Part I: applications, *ASME Journal of Dynamic Systems, Measurements, and Control* 106 (4) (1984) 249–254.

[20] D.A. Turcic, A. Midha, Dynamic analysis of elastic mechanism systems Part II: experimental results, *ASME Journal of Dynamic Systems, Measurements, and Control* 106 (4) (1984) 255–260.

[21] F.W. Liou, A.G. Erdman, Analysis of a high-speed flexible four-bar linkage: Part I-formulation and solution, *ASME Journal of Vibration and Acoustics* 111 (1) (1989) 35–41.

[22] Y. Wang, Z.P. Wang, A time finite element method for dynamic analysis of elastic mechanisms in link coordinate systems, *Computers & Structures* 79 (2) (2001) 223–230.

[23] S.D. Yu, W.L. Cleghorn, Dynamic instability analysis of high-speed flexible four-bar mechanisms, *Mechanism and Machine Theory* 37 (11) (2002) 1261–1285.

[24] S.D. Yu, F. Xi, Free vibration analysis of planar flexible mechanisms, *ASME Journal of Mechanical Design* 125 (4) (2003) 764–772.

[25] Z.J. Yang, J.P. Sadler, Large-displacement finite element analysis of flexible linkages, *ASME Journal of Mechanical Design* 112 (2) (1990) 175–181.

[26] M. Hać, Dynamic of planar flexible mechanisms by finite element method with truss-type elements, *Computers & Structures* 39 (1–2) (1991) 135–140.

[27] T.S. Liu, J.C. Lin, Forced vibration of flexible body systems: a dynamic stiffness method, *ASME Journal of Vibration and Acoustics* 115 (4) (1993) 468–476.

[28] M. Benati, A. Morro, Formulation of equation of motion for a chain of flexible links using Hamilton's principle, *ASME Journal of Dynamic Systems, Measurements, and Control* 116 (1) (1994) 81–88.

[29] R. Caracciolo, D. Richiedei, A. Trevisani, Design and experimental validation of piecewise-linear state observers for flexible link mechanisms, *Meccanica* 41 (6) (2006) 623–637.

[30] W.J. Book, Recursive Lagrangian dynamics of flexible manipulator arms, *The International Journal of Robotics Research* 3 (3) (1984) 87–101.

[31] P.B. Usuro, R. Nadira, S.S. Mahil, A finite element/Lagrange approach to modeling lightweight flexible manipulators, *ASME Journal of Dynamic Systems, Measurements, and Control* 108 (3) (1986) 198–205.

[32] S. Nagarajan, D.A. Turcic, Lagrangian formulation of the equations of motion for elastic mechanisms with mutual dependence between rigid body and elastic motions Part I: element level equations, *ASME Journal of Dynamic Systems, Measurements, and Control* 112 (2) (1990) 203–214.
[33] S. Nagarajan, D.A. Turcic, Lagrangian formulation of the equations of motion for elastic mechanisms with mutual dependence between rigid body and elastic motions Part II: system equations, *ASME Journal of Dynamic Systems, Measurements, and Control* 112 (2) (1990) 215–224.
[34] X.M. Zhang, H.Z. Liu, Y.W. Shen, Finite dynamic element analysis for high-speed flexible linkage mechanisms, *Computers & Structures* 60 (5) (1996) 787–796.
[35] S.Q. Yuan, Q.Y. Xu, L. Zhang, Experiments on active vibration control of a flexible four-bar linkage mechanism, *ASME Journal of Vibration and Acoustics* 122 (1) (2000) 82–92.
[36] R. Caracciolo, A. Trevisani, Simultaneous rigid-body motion and vibration control of flexible four-bar linkage, *Mechanism and Machine Theory* 36 (2) (2001) 221–243.
[37] Y.M. Song, C. Zhang, Y.Q. Yu, Neural networks based active vibration control of flexible linkage mechanism, *ASME Journal of Mechanical Design* 123 (2) (2001) 266–271.
[38] X.M. Zhang, C.J. Shao, A.G. Erdman, Active vibration controller design and comparison study of flexible linkage mechanism systems, *Mechanism and Machine Theory* 37 (9) (2002) 985–997.
[39] A. Trevisani, Feedback control of flexible four-bar linkages: a numerical and experimental investigation, *ASME Journal of Sound and Vibration* 268 (5) (2003) 947–970.
[40] X.M. Zhang, J.W. Lu, Y.W. Shen, Active noise control of flexible linkage mechanism with piezoelectric actuators, *Computers & Structures* 81 (20) (2003) 2045–2051.
[41] X.M. Zhang, A.G. Erdman, Dynamic responses of flexible linkage mechanisms with viscoelastic constrained layer damping treatment, *Computers & Structures* 79 (13) (2001) 1265–1274.
[42] X.M. Zhang, Complex mode dynamic analysis of flexible mechanism systems with piezoelectric sensors, *Multibody System Dynamics* 8 (1) (2002) 51–70.
[43] C.W. King, M.I. Campbell, J.J. Beaman, S.V. Streenivasan, Synthesis of multistable equilibrium linkage systems using an optimization approach, *Structural and Multidisciplinary Optimization* 29 (6) (2005) 477–487.
[44] X.M. Zhang, A.G. Erdman, Optimal placement of piezoelectric sensors and actuators for controlled flexible linkage mechanisms, *ASME Journal of Vibration Acoustics* 128 (2) (2006) 256–260.
[45] L. Luo, S.G. Wang, J.Q. Mo, J.G. Cai, On the modeling and composite control of flexible parallel mechanism, *The Internal Journal of Advanced Manufacturing Technology* 29 (7–8) (2006) 786–793.
[46] R. Żbikowski, G. Galiński, C.B. Pedersen, Four-bar linkage mechanism for insect like flapping wings in hover: concept and an outline of its realization, *ASME Journal of Mechanical Design* 127 (4) (2005) 817–824.
[47] B. Yardimoglu, T. Yildirim, Finite element model for vibration analysis of pre-twisted Timoshenko beam, *Journal of Sound and Vibration* 273 (4–5) (2004) 741–754.
[48] H. Antes, M. Schanz, S. Alvvermann, Dynamic analyses of plane frames by integral equations for bars and Timoshenko beams, *Journal of Sound and Vibration* 276 (3–5) (2004) 807–836.
[49] N.M. Auciello, A. Ercolano, A general solution for dynamic response of axially loaded non-uniform Timoshenko beams, *International Journal of Solids and Structures* 41 (18–19) (2004) 4861–4874.
[50] Y. Urthaler, J.N. Reddy, A corotational finite element formulation for the analysis of planar beams, *Communications in Numerical Methods in Engineering* 21 (10) (2005) 553–570.
[51] E. Viola, P. Ricci, M.H. Aliabadi, Free vibration analysis of axially loaded cracked Timoshenko beam structures using the dynamic stiffness method, *Journal of Sound and Vibration* 304 (1–2) (2007) 124–153.
[52] S. Yuan, K. Ye, C. Xiao, F.W. Williams, D.K. Kennedy, Exact dynamic stiffness method for non-uniform Timoshenko beam vibrations and Bernoulli–Euler column buckling, *Journal of Sound and Vibration* 303 (3–5) (2007) 526–537.
[53] E. Manoach, P. Ribeiro, Coupled, thermoelastic, large amplitude vibrations of Timoshenko beams, *International Journal of Mechanical Sciences* 46 (11) (2004) 1589–1606.
[54] S.R. Li, Y.H. Zhou, Geometrically nonlinear analysis of Timoshenko beams under thermomechanical loadings, *Journal of Thermal Stresses* 26 (9) (2003) 861–872.
[55] S.R. Li, S. Xi, Large thermal deflections of Timoshenko beams under transversely non-uniform temperature rise, *Mechanics Research Communications* 33 (1) (2006) 84–92.
[56] Y.X. Zhang, M.A. Bradford, Nonlinear analysis of moderately thick reinforced concrete slabs at elevated temperatures using a rectangular layered plate element with Timoshenko beam functions, *Engineering Structures* 29 (10) (2007) 2751–2761.
[57] J.S. Przemieniecki, *Theory of Matrix Structural Analysis*, McGraw-Hill, New York, 1976.
[58] J.L. Nowinski, *Theory of Thermoelasticity with Applications*, Sijthoff & Noordhoff, Netherlands, 1978.
[59] D.J. Dawe, A finite element for the vibration analysis of Timoshenko beams, *Journal of Sound and Vibration* 60 (1) (1978) 11–20.
[60] I.H. Shames, C.L. Dym, *Energy and Finite Element Methods in Structural Mechanics*, Hemisphere, New York, 1985.
[61] A.H. Roger, R.J. Charles, *Matrix Analysis*, Cambridge, New York, 1985.
[62] A. Midha, A.G. Erdman, A closed-form numerical algorithm for the periodic response of high-speed elastic linkage, *ASME Journal of Engineering for Industry* 101 (1) (1979) 154–162.
[63] F.P. Incropera, D.P. DeWitt, T.L. Bergaman, A.S. Lavine, *Fundamentals of Heat and Mass Transfer*, sixth ed, Wiley, New York, 2006.